Desalination and Water Treatment
www.deswater.com
doi: 10.5004/dwt.2020.26307

206 (2020) 429–438
December

Identification and use of local iron-ores deposit as adsorbent: adsorption study and photochemical regeneration

Selma Khelifi[a], Abderrahim Choukchou-Braham[b], Mohamed Habib Oueslati[c], Hassen M. Sbihi[d], Fadhila Ayari[a,*]

[a]*LR 05/ES09 Laboratory of Applications of Chemistry to Resources and Natural Substances and to the Environment (LACReSNE), Faculty of Sciences of Bizerte, University of Carthage, Zarzouna 7021, Tunisia, emails: fadhilaayari@yahoo.fr (F. Ayari), selma.khelifi@gmail.com (S. Khelifi)*
[b]*Laboratoire de Catalyse et Synthèse en Chimie Organique (LCSCO), Université de Tlemcen, Tlemcen 13000, Algérie, email: cba_dz@yahoo.fr (A. Choukchou-Braham)*
[c]*Department of Chemistry, Preparatory Institute for Scientific and Technical Studies, Carthage University, P.O. Box: 51, Marsa 2070, Tunisia, email: oueshabib@yahoo.fr (M.H. Oueslati)*
[d]*Chemistry Department, College of Science, King Saud University, P.O. Box: 2454, Riyadh 1145, Saudi Arabia, email: adam.sbihi@yahoo.com (H.M. Sbihi)*

Received 14 February 2020; Accepted 2 July 2020

ABSTRACT

Natural iron oxide (TIO) was prepared and investigated as an adsorbent for diazo dye (Congo Red, CR) removal. Characterization, adsorption capacity, and photochemical regeneration of the adsorbent were studied. Results show that the optimal adsorption condition are [CR] = 10^{-4} M, adsorbent dose = 0.1 g, pH = 7, and contact time = 60 min. 60 min was sufficient to reach adsorption equilibrium with 80% of Congo red removal. Adsorption process obeyed Langmuir type and pseudo-second-order kinetic suggested monolayer adsorption and physisorption process. Results show that advanced oxidation process via photo-Fenton reaction, carried out at neutral pH under UV light irradiations allowed the restitution of the used catalyst (TIO). Ninety minutes is required for photochemical regeneration of saturated adsorbent, the regeneration efficiency can reach 96% under the optimal proposed conditions (25°C, [H_2O_2] = 10 mmol L^{-1}, [CR] = 10^{-4} mol L^{-1}) at neutral pH and under UV irradiations. After 3 consecutive adsorption–regeneration cycles, the regeneration efficiency was still achieved (96%) and the adsorbent has a good stability with the increase of experimental runs.

Keywords: Adsorption; Local material; Congo Red; Regeneration, photo-Fenton; Wastewater treatment

1. Introduction

Overconsumption of clothing has a considerable impact on our planet. Materials used and wastes are all factors that make the textile industry a major contributor to environmental pollution. However, substances from textiles discharged in water course, sea, and river during the manufacture of the clothes are often toxic for our health [1]. Wastewater contains a lot of toxic products that harm flora and fauna and are potential source causing cancer [2]. Among these pollutants, dyes which are very used in the textile industry and generated wastewater contains a high concentration of these chemical compounds. So, textile manufacturers must minimize toxic products, such as additives, organic compounds, dyes, etc., from their wastewater to accepted standards before releasing it into waterways [3].

Ozonation, electrocoagulation, biological process, and reverse osmosis process are physical and chemical techniques used to treat textile wastewater [4–7]. However, they are

* Corresponding author.

often expensive, ineffective, and cause secondary pollution because pollutant was just transferred from one phase to another phase [8]. Among removal technologies proposed for the treatment of dye-containing wastewater, adsorption has been suggested as an effective and affordable method according to some researchers in this field [9,10].

Adsorption method is a high effective separation technique and it is considered the best among the other techniques for wastewater purification in term of cost, simplicity, and insensitive to toxic substances [11]. Adsorption occurs between two phases: liquid–liquid, gas–liquid, and liquid–solid interfaces. For this reason, many adsorbents were used and applied in water purification according to Lorenc-Grabowska and Gryglewicz [12]. Among these adsorbents, commercial activated carbon is widely used by several operators. Although, it is known by the high cost [13].

Wherefore, researchers are currently interested in natural materials; abundant and inexpensive.

For that, eco-friendly materials such as clay mineral [14], sepiolite [15], and waste mussel shells [16], due to their abundance and availability, also according to their physico-chemical properties, are emerging as alternative and potential adsorbents for the removal of polluted organic products.

In this context, several Tunisian resources can be of considerable interest in adsorption process like natural iron oxide (TIO), which is commonly found in the metal ore mines, has been already used for the treatment of polluted water, since low amount of iron is leached and because pH control of the water/wastewater can be avoided [17]. Bel Hadjltaief et al. [18] in their study describe the removal of 4-chlorophenol from wastewater by locally hematite and siderite. Mined pyrite also chalcopyrite from Jendouba (north Tunisia) have been used by Ltaïef et al. [19] as catalysts for the removal of Tyrosol. Yet, the writings are still restricted to these topic reports with these deposits. However, iron deposits from Nefza region were not conquered up till now, as water decontamination.

For all that, adsorption technique was considered a storage method of the pollutant. It's just transfer the dye from one phase to another without destruction of molecules [20]. For this reason regeneration of the studied adsorbent was carried out via photochemical route under UV light irradiation in order to evade the storage of the toxic product from the liquid phase to the solid adsorbent.

In this investigation, we show for the first time that this material: iron deposit from the area of Tamra (northern Tunisia) can be used as adsorbent for the removal of organic pollutants. In this sense, the main objective of the present work is to study the activity of raw Tunisian deposit (iron oxide) in the adsorption of azo dye in aqueous solution followed by photo-Fenton regeneration of the adsorbent and mineralization of dye.

2. Experimental details

2.1. Materials and products

2.1.1. Adsorbate and other chemicals

All chemicals used in this work were of analytical grade and used without any further purification. Model pollutant is an anionic secondary azo dye: Congo Red ($C_{32}H_{24}N_6O_6S_2$).

Depending on the acidity of the medium it changes its color and therefore chemical structure; Red at pH ≥ 6, and blue at pH < 5.5 [21, 22]. Its pKa is close to 3.7 [23]. The cationic and anionic forms are presented in Fig. 1.

2.1.2. Presentation of investigated material

2.1.2.1. Localization of the studied iron ore deposit

Material used in this study is iron oxide taken from the deposit located in the northeast of the Nefza region (Northwestern of Tunisia) (Fig. 2). This deposit belongs to the Tamra Basin. The Nefza area has deposits rich in metals (Fe, Pb, and Zn) and is a mining center in northern Tunisia [24, 25]. Tamra region contains active iron mines that are very rich in hematite and goethite ores. Also, an interesting

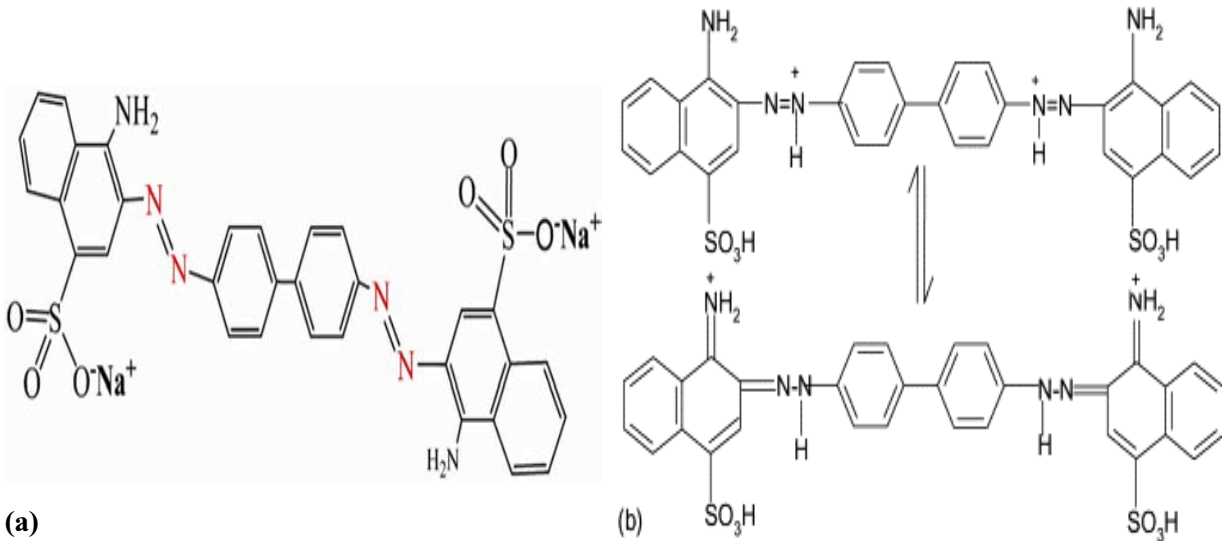

Fig. 1. Anionic form of CR(a) and cationic form of CR(b).

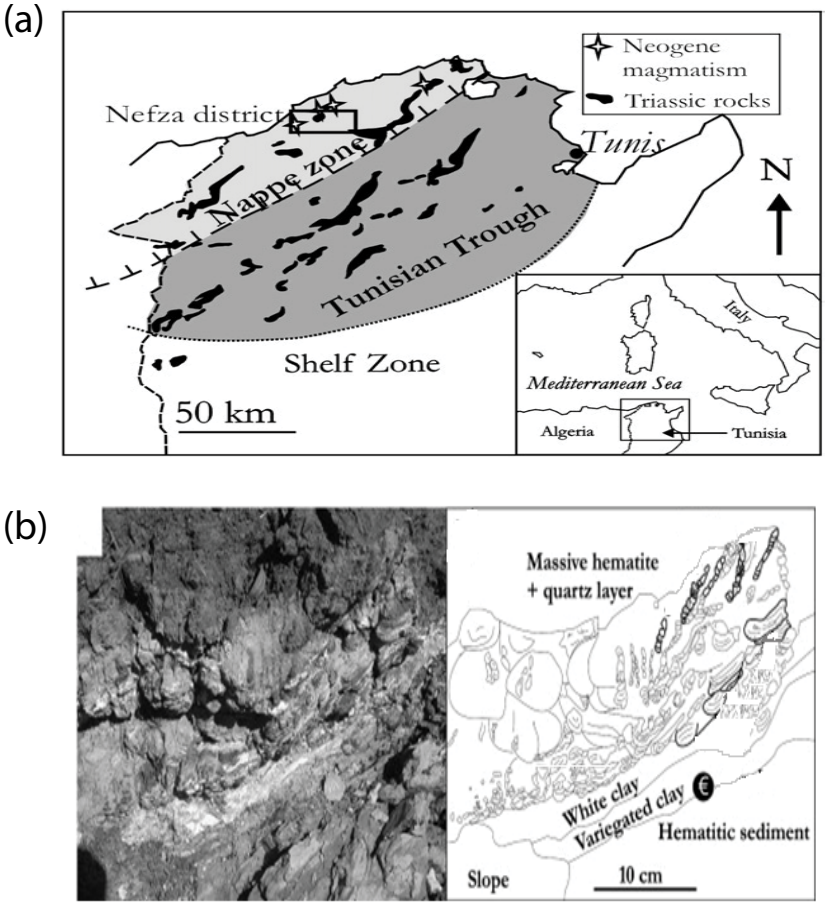

Fig. 2 (a) Geographic location of Nefza region [27, 28], and (b) clay and iron deposits into Tamra district with schematic drawing accentuating diverse natures of iron and clay phase [25].

Halloysite clay deposit is located at the top of its litho-stratigraphic series. Variation and richness of deposits in the northern zone of Nefza results from the association of various large tectonic, allochthonous, and autochthonous phases [26].

2.1.2.2. Preliminary preparation of iron oxide sample

Raw iron oxide contains some solid impurities which can affect the adsorptive property. Removing the solid impurities thoroughly is a necessary step before adsorption study. For this reason, the set of iron oxide sample (yellowish color) was crushed and sieved and the fraction less than 63 μm was recovered. Homogeneous sample obtained will be noted later in the work by Tamra iron ore (TIO).

2.1.2.3. Characterization

Chemical composition of iron oxide was determined by X-ray fluorescence spectrometer (XRF) using a commercial instrument (ARL 9900 of THERMOFISCER, USA), using monochromatic radiation $K_{\alpha 1}$ of cobalt (λ = 1.788996 Å). Powder X-ray diffraction (PXRD) pattern of the sample was obtained from 2° to 80° range by the diffractometer (PANalytical X'Pert HighScore plus diffractometer, Malvern) with monochromatic radiation CuK_{α} (λ = 1.5406 Å). Isotherm of nitrogen adsorption–desorption of material was measured using Quantachrome model Nova 1000^{e} surface and porosity analyzer. The specific surface area (S_{BET}) was obtained by the Brunauer–Emmett–Teller (BET) method and the total pore volume (V_t) was calculated at a relative N_2 pressure of P/P_0 = 0.99 at liquid nitrogen temperature of 196°C. Pore size distribution in the mesopore range was calculated using the Barrett–Joyner–Halenda (BJH) method based on the desorption arm of the isotherm. Fourier transform infrared (FTIR) spectroscopic data was determined using Perkin Elmer 783 dispersive spectrometer in the range of 4,000–400 cm^{-1}. Zetasizer (nano Z_S) was used to obtain zeta potential value of the sample at different pH values in order to determine their points of zero charge (pH_{pzc}). Optical properties of sample were monitored by UV-vis diffuse reflectance method using UV-visible spectrophotometer (Shimadzu UV-2700). Time-resolved photoluminescence (PL) was performed on a FLS980 spectrometer by applying laser excitation at 400 nm.

2.2. Adsorption treatment of CR wastewater

Adsorption of Congo Red by TIO was investigated by experiments in batch mode. An appropriate amount of adsorbent was suspended into 50 mL of 10^{-4} mol L^{-1} CR

aqueous solution and then mixed by shaking (T = 25°C) at appropriate pH. Adsorbent and adsorbate were separated through centrifugation and filtration, remaining dye amount was measured spectrophotometrically using UV-vis spectrophotometer (Shimadzu Model Perkin Elmer, Kyoto, Japan). The absorbance was monitored at 497 nm in basic and neutral medium and at 562 nm in the acid medium (pH < 5.5). The rate of the adsorbed dye was determined [Eq. (1)]:

$$\% \text{ RE} = \frac{C_0 - C_t}{C_0} \times 100 \quad (1)$$

The adsorption capacity (Q_{ads}) was calculated using Eq. (2):

$$Q_{ads} = \frac{\left(C_0 - C_t\right)}{m} V \quad (2)$$

where C_0 is the dye amount at t = 0, C_t is the dye amount at $t \neq 0$, m is the quantity of the used TIO (g), and V is the volume of dye solution (L).

2.3. Photo-Fenton study to regenerate the adsorbent

Photo-Fenton experiments were performed to achieve the regeneration of the TIO adsorbent after adsorption study. All experiments were carried out at room temperature (T = 25°C) in a cylindrical photoreactor equipped with a 125 W Philips HPK UV-lamp (UV-A) placed in a plugging tube. A pyrex cylindrical jacket located around the plugging tube allows irradiation with wavelengths of around λ = 350 nm. Congo red dye was oxidized by H_2O_2 using TIO as photo-Fenton heterogeneous catalyst. The initial concentration of CR was 10^{-4} mol L^{-1} and the total volume of the reaction solution was 150 mL. First of all 100 mg of TIO was mixed with 0.15 L of CR, agitated 60 min to attain an equilibrium, then the mixture was irradiated below UV light and at specified period, 3 mL of the treated solution was sampled and centrifuged. Absorbance of the supernatant was measured using UV-visible spectrophotometer. Changes in this parameter suggest a change in the residual amount of CR. At the end of the experiment, dye mineralization was confirmed using ion chromatography analysis by the quantification of NO_3^- and SO_4^{2-} ions. All analyses were conducted with a metrosop A Supp 4 anionic column at 40°C using a mobile phase composed of 1.8 mM Na_2CO_3 and 1.7 mM $NaHCO_3$ at 1 mL min^{-1}. The Fe ions leaching from the adsorbent were measured using a 1300 Perkin Elmer (Waltham, USA) atomic absorption spectrophotometer.

3. Results and discussion

3.1. Characterization of adsorbent

TIO sample was identified via XRF spectrometer, results show that the major constituents of this material were: Fe_2O_3 (59.76%), CaO (4.87%), SiO_2 (15.38%), Al_2O_3 (5.03%), MnO (2.08%), Cr_2O_3 (0.02%), and MgO (0.77%). Iron oxide was the most important constituent of TIO. Alumina (Al_2O_3) and silica (SiO_2) were normally ascribed to kaolinite phase. Also, worth noting is this natural material contains some heavy metals.

X-ray diffractogram (Fig. 3) shows that the principal phases constitute this sample are goethite FeOOH, magnetite Fe_3O_4, and hematite Fe_2O_3 confirmed by the presence of their appropriate peaks (crystal planes).

The infrared spectrum of TIO (Fig. 4) shows the characteristic absorption bands of a hydroxyl group in goethite (Fe–OH), particularly at about 894 and 797 cm^{-1} [29]. The bands at 476, 538, and 600 cm^{-1} are related to the symmetric stretching vibration bands of Si–O/Al–O and O–Fe–O, respectively [30]. The peaks at about 1,046 and 1,656 cm^{-1} are assigned to the asymmetric stretching vibration of Fe–O–Si and O–H groups, respectively. Band at around 3,300 cm^{-1} was attributed to the hydrogen-bonded hydroxyl groups [29]. Hematite phase was characterized by these two characteristic bands: 476 and 538 cm^{-1} [30].

Porosity of the sample was probed by N_2 adsorption–desorption studies. Optimum porosity and high surface area are essential characteristics for an efficient adsorbent material [31]. Hence, BET surface area, pore volume, average pore diameter, and pore size of TIO sample, were measured (Table 1). Results show that TIO exhibits an important surface area and porosity. These significant values of can be helpful in the adsorption process by providing

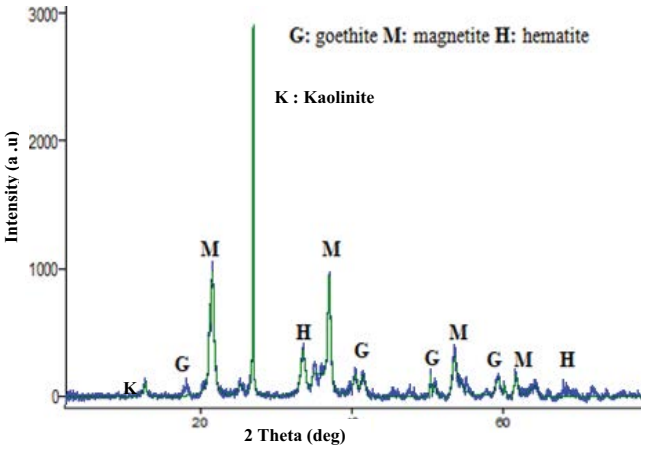

Fig. 3. X-ray diffractogram of TIO.

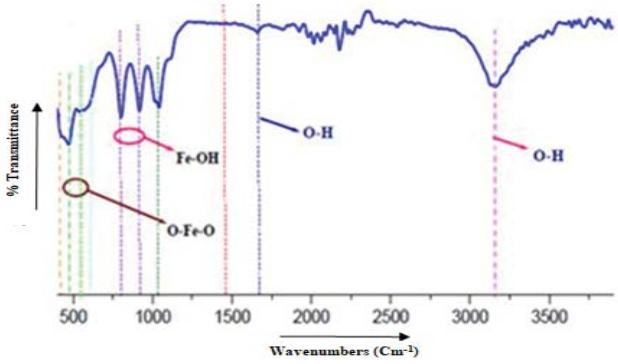

Fig. 4. Infrared spectrum of TIO.

Table 1
Textural properties of TIO sample

S_{BET} ($m^2\ g^{-1}$)	44
V_p ($cm^3\ g^{-1}$)	0.11
$S_{BJH/mesp}$ ($m^2\ g^{-1}$)	35.17
$V_{BJH/mesp}$ ($cm^3\ g^{-1}$)	0.096
S_{micr} ($m^2\ g^{-1}$)	0
V_{micr} ($cm^3\ g^{-1}$)	0
D (Å)	19.1

enhanced interfacial contact among dye molecules and adsorbent surface. Obtained isotherm (Fig. 5) is a type IV isotherm with a hysteresis loop [32]. Tamra iron show fine pore size distribution (Fig. 5) in the range of 2 nm suggested that it is microporous materials.

Zeta potential of the TIO material at different pH is shown in Fig. 6a. The pH of zero charge (pH_{PZC}) of TIO is determined as 7, signifying that surface charge is positive at pH < pH_{PZC} and negative at pH > pH_{PZC}. UV-vis diffuse reflectance spectra of TIO (Fig. 6b), shows that this material display two remarkable edges absorption toward λ = 600 and 760 nm. This result indicated that the optical response of TIO was wholesale into visible light domain. According to Tanwar et al. [33], this optical domain can be very useful to achieve the photocatalytic activity.

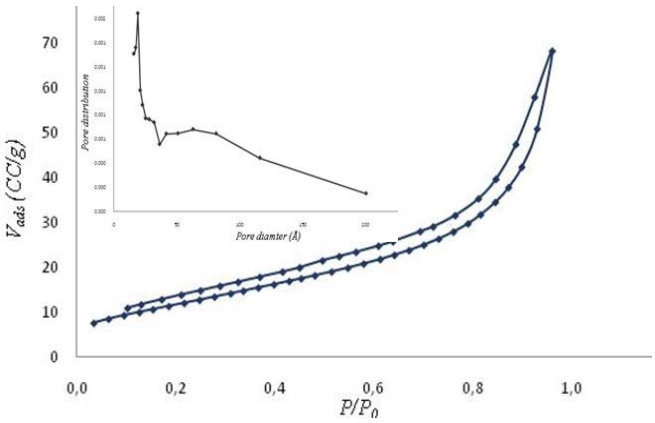

Fig. 5. Adsorption–desorption isotherm (in set) BJH-method pore size distribution curve from nitrogen sorption of TIO sample.

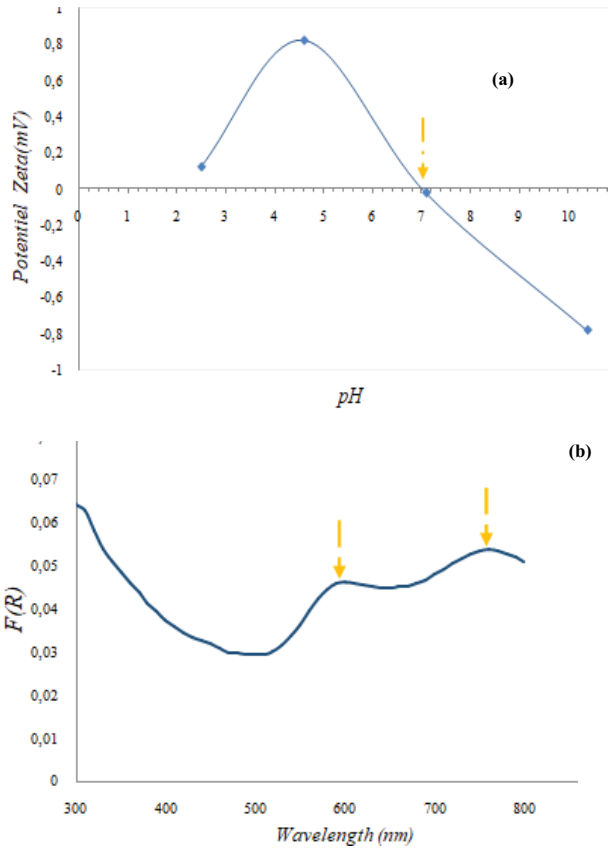

Fig. 6. (a) Zeta potential of TIO and (b) UV-solid diffuse reflectance.

3.2. Adsorption study

3.2.1. Optimization strategy

Effect of the influential parameter on CR dye adsorption was evaluated; the adsorption tests were done over a pH range of 4–9, at different initial dye concentration (13.9–696.96 mg L^{-1}) and contact time (10–90 min).

3.2.1.1. Effect of contact time

The study of the adsorbent/adsorbate contact time is an imperative factor for determining the saturation time at equilibrium and obviously the desorption time. Operating conditions considered for this study are as follows: 0.1 g of TIO; 10^{-4} M of CR at pH = 7 and 25°C. Fig. 7 represents the evolution of the CR adsorbed quantity during its adsorption on the natural adsorbent TIO. As can be seen, equilibrium adsorption was achieved around 1h of adsorbent/adsorbate contact. The % adsorption is 80% in 60 min. It should be noted from this kinetic study that 60 min is a sufficient period to establish the adsorption–desorption equilibrium by this adsorbent.

3.2.1.2. Effect of initial dye concentration

The effect of the initial dye concentration (C_i) on its percentage of adsorption by TIO (adsorbent) was studied for C_i ranging from 13.9 to 696.96 mg L^{-1}, this study was carried out at neutral pH, room temperature, and a mass of TIO equal to 0.1 g.

As can be seen in Fig. 8a, when C_i increases the percent of dye adsorption gradually diminished from 95.62% to 52.5%. This is explained by the drop off in the number of adsorption sites toward the number of CR molecules in the solution. Which so-called the saturation [34].

3.2.1.3. Effect of pH

Since pH medium is an important parameter that affects adsorbent and/or adsorbate structure consequently the rate of adsorbate removal and as CR structure is pH

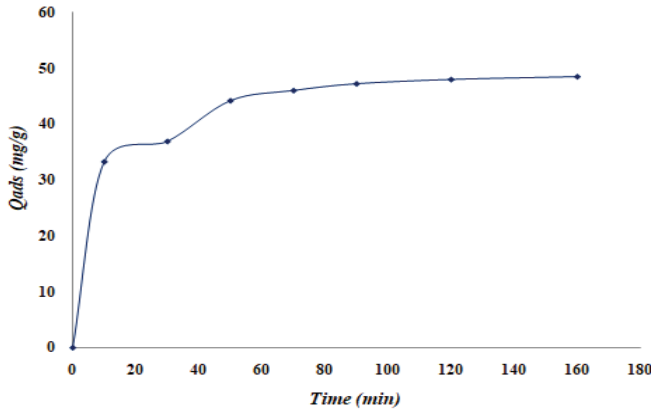

Fig. 7. Adsorption kinetics of CR onto TIO.

depending [35, 36], it changes from cationic form CR^+ (pH < 5,5) to basic form CR^- (pH > 5,5), in this circumstance the effect of pH was studied from acid medium to basic medium (2 ≤ pH ≤ 12), Fig. 8 shows the different CR structures in aqueous solution at various pH.

Results show that at pH = pH_{PZC} of TIO (pH_{PZC} = 7 Fig. 6) adsorption of CR was favorable (Fig. 8b) the rate of adsorption can reach 80%, since the surface of TIO develops a positive charge density at this pH and the dye was in its anionic form. However at pH > pH_{PZC} we notice a sharp decrease in the retention rate of CR, explained by the repulsion between CR^- and HO^- (charge density of TIO is highly negative). At pH < pH_{PZC} adsorption of CR by TIO is also lower since at this pH medium the dye is as its cationic form (CR^+) and the adsorbent develop a positive charge density.

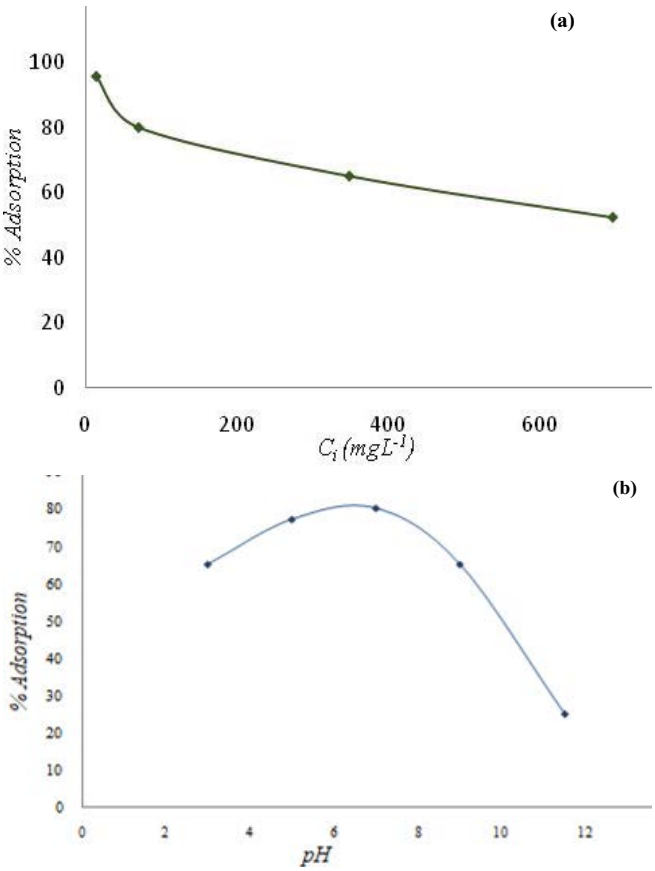

Fig. 8. (a) Effect initial dye amount and (b) initial pH onto dye sorption.

3.2.2. Kinetics modeling

In order to examine the adsorption process of CR onto this adsorbent, pseudo-first-order and pseudo-second-order models are used to test the experimental data and to predict the mechanism involved in the sorption process. The kinetics data were analyzed based on the regression coefficient R^2 and the amount of dye removal at equilibrium (Fig. 9, Table 2).

The pseudo-second-order model fit very well with the experimental results of CR dye adsorption onto TIO (R^2 = 1; Fig. 9b), which suggests a physisorption process.

3.3. Adsorption isotherms

According to Giles classification [37], adsorption isotherm (Fig. 10a) of CR dye by this natural adsorbent is of *L* type, signaling monolayer adsorption with a retention percent reaching at saturation 172.82 mg g^{-1}. This result confirms the good adsorption property of this material.

3.4. Isotherm modeling

There are several adsorption models that explain the experimental equilibrium results. Langmuir [38] and Freundlich [39] isotherm models were used to describe the CR adsorption behavior onto the natural adsorbent TIO. The nonlinear equations for each isotherm model are presented as follows:

Langmuir isotherm model:

$$q_e = \frac{q_m K_L C_e}{1 + K_L C_e} \tag{3}$$

where q_m is the maximum monolayer adsorption capacity (mg g^{-1}), C_e is the amount of residual dye at equilibrium (mg L^{-1}), and K_L is the Langmuir constant (L mg^{-1}).

Freundlich isotherm model:

$$q_e = K_F C_e^{1/n} \tag{4}$$

where q_e is the mass concentration of CR adsorbed (mg g^{-1}), C_e is the amount of residual CR at equilibrium (mg L^{-1}), K_F is the is a measure of adsorption capacity, and n is an indicator of adsorption effectiveness.

Results show that the Langmuir model concord very well with experimental data (Fig. 10b), Figure of Freundlich model not presented) since the value of the correlation coefficient R^2 is very close to unity (R^2 = 0.983, Table 3). Hence adsorption sites of TIO are homogeneous and uniform and the adsorption process is of a monolayer type [38]. The resulting maximum adsorption capacity and Langmuir adsorption constant were calculated to be 55.55 mg g^{-1} and 0.30 L mg^{-1}, respectively.

Table 2
Kinetics parameters of CR dye adsorption onto Tamra iron ore

Model	Equation	Parameters	Values
Pseudo-first-order	$\mathrm{Ln}(q_e - q_t) = \mathrm{Ln}\, q_e - K_1 t$ (3) [33]	Q_e (mg.g^{-1})	34.61
		K_1 (min^{-1})	0.042
		R^2	0.889
Pseudo-second-order	$\frac{t}{q_t} = \frac{1}{K_2 q_e^2} + \frac{1}{q_e} t$ (4) [34]	Q_e (mg.g^{-1})	52.63
		K_2 (g mg^{-1}min^{-1})	0.002
		R^2	0.995

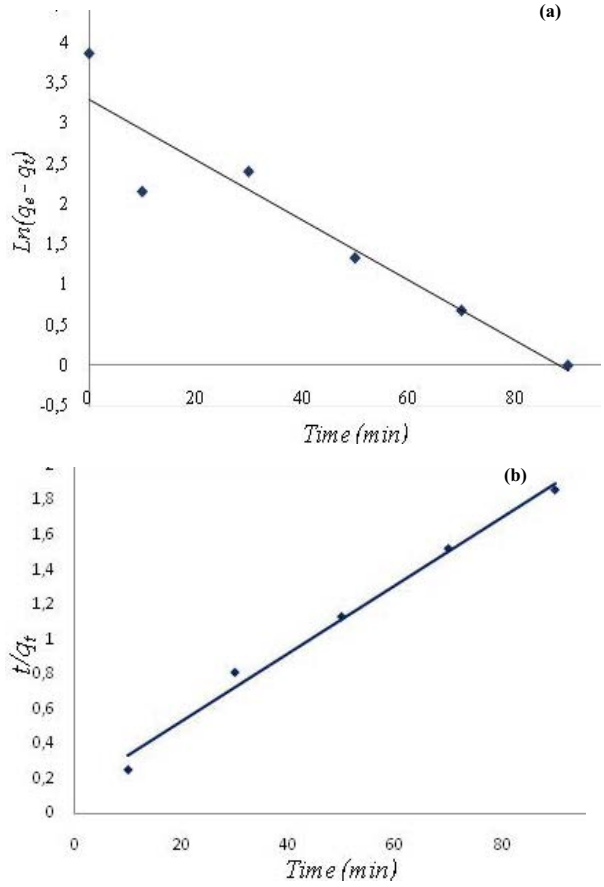

Fig. 9. Kinetic study (a) pseudo-first-order and (b) pseudo-second-order models.

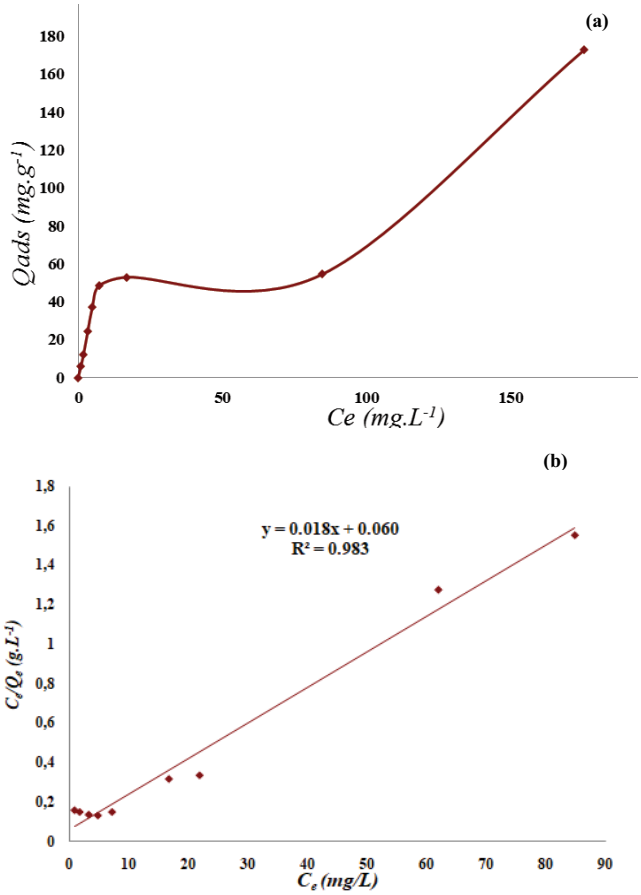

Fig. 10. (a) Adsorption isotherm of CR onto TIO material and (b) modelization according to Langmuir model.

3.5. Adsorbent regeneration

Regeneration/reusability as well and adsorbent's stability are the most important commercial features in the water treatment process. The regeneration of TIO material was performed by Fenton and photo-Fenton oxidation. The procedure consists in oxidizing the CR dye stored on the surface of the adsorbent TIO through photochemical route using hydrogen peroxide (H_2O_2) as oxidant agent, TIO as catalyst because of iron content, CR as pollutant, and UV irradiations as light source.

3.5.1. Fenton and Photo-Fenton regeneration

Heterogeneous Fenton reaction in dark and under UV light irradiation was monitored after 60 min of adsorption equilibrium using 10^{-4} mol L^{-1} as initial concentration of CR dye, 0.1 g as adsorbent dose and 10 mmol L^{-1} as H_2O_2 concentration. As shown in Fig. 11, CR dye removal efficiency reached about 97% after 240 min in the dark and 100% under UV irradiation in 10 min of irradiation.

Mineralization of CR dye is important to confirm the adsorbent regeneration. According to Eq. (5), the total

Table 3
Isotherm modeling of CR dye adsorption onto Tamra iron ores adsorbent

Isotherms	Parameters	Values
Langmuir	Q_{max} (mg g^{-1})	55.55
	K_L (L mg^{-1})	0.30
	R^2	0.983
Freundlich	K_F	10.77
	n	1.95
	R^2	0.827

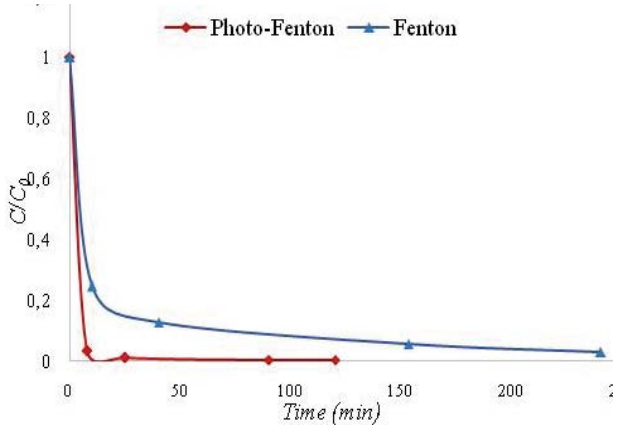

Fig. 11. Oxidation efficiency of CR dye in dark (Fenton) and under UV light irradiations (photo-Fenton) ($[CR]_0 = 10^{-4}$ mol L^{-1}, $[H_2O_2]_0 = 10$ mmol L^{-1}, $pH_0 = 7$, and $T = 25$°C).

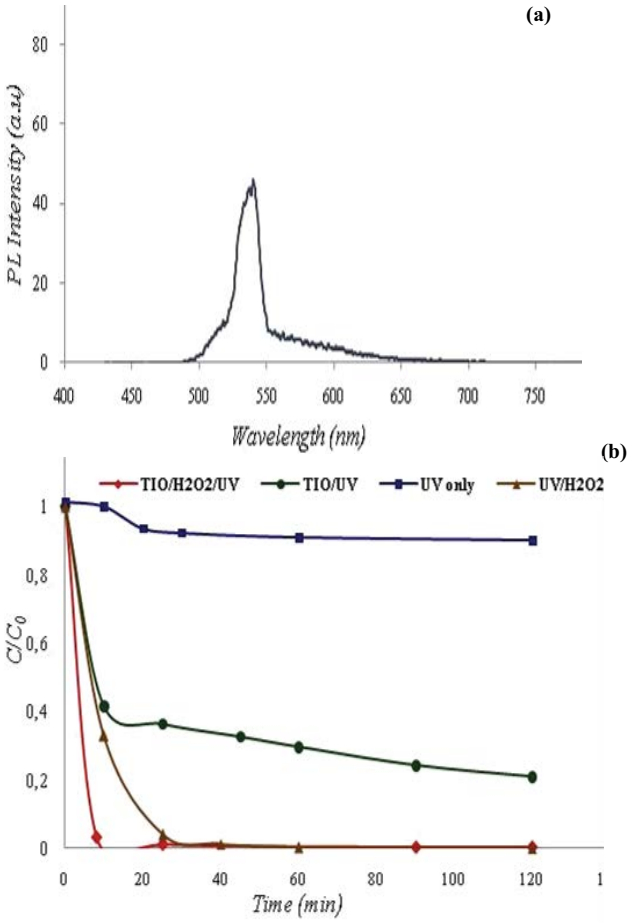

Fig. 12. (a) Adsorbent regeneration under different condition: (TIO/UV), (TIO/H_2O_2/UV), (UV/H_2O_2), (UV only), and (b) photo-luminescence spectra excited at 400 nm of TIO material.

mineralization of CR under these conditions allows to obtain SO_4^{2-}, NO_3^-, CO_2, and H_2O as final products.

$$C_{32}H_{22}N_6Na_2O_6S_2 + 91\ H_2O_2 \leftrightarrow 32CO_2 + 98\ H_2O + 6NO_3^- + 2SO_4^{2-} + 2Na^+ + 8H^+ \quad (5)$$

Accordingly, ionic chromatography analysis was conducted at the end of the reaction for sulfate SO_4^{2-} quantification. Obtained results were mentioned in Table 4. As can be seen, in the dark condition the mineralization efficiency of CR dye is only 60% which is enhanced to 99% under UV irradiation. The above results clearly reveal that UV irradiations enhance CR dye mineralization and the regeneration of TIO adsorbent.

For a better explanation of the photochemical regeneration of the investigated material, photocatalytic degradation of CR dye was conducted under the different condition in order to evaluate their contribution in photo-Fenton reaction. As can be shown in Fig. 12a, CR dye cannot be affected by UV light irradiation alone. In the case of UV light irradiation combined with H_2O_2 (UV/H_2O_2), CR removal efficiency was 98% because UV light catalyzed H_2O_2 to generate the HO· radicals according to Eq. (6) but mineralization percent is only 15%.

$$H_2O_2 + h\nu \rightarrow 2HO\cdot \quad (6)$$

Also with the system UV/TIO, the removal efficiency achieved 76% within 120 min and in the contrary mineralization percent reached 71%, because of a significant absorption of photons by the iron particles in the suspension, even

Table 4
Mineralization results of CR adsorbent after photo-Fenton regeneration of TIO

Process	% Removal	$[SO_4^{2-}]$ (mg L^{-1})	$[NO_3^-]$ (mg L^{-1})	% Mineralization	$[Fe^{3+}]$ (mg L^{-1})
Fenton (TIO/H_2O_2)	97	11.47	0.055	60	0.28
Photo-Fenton (TIO/H_2O_2/UV)	100	19.09	0.16	99	3.2
(TIO/UV)	76	13.69	0.013	71	1.75

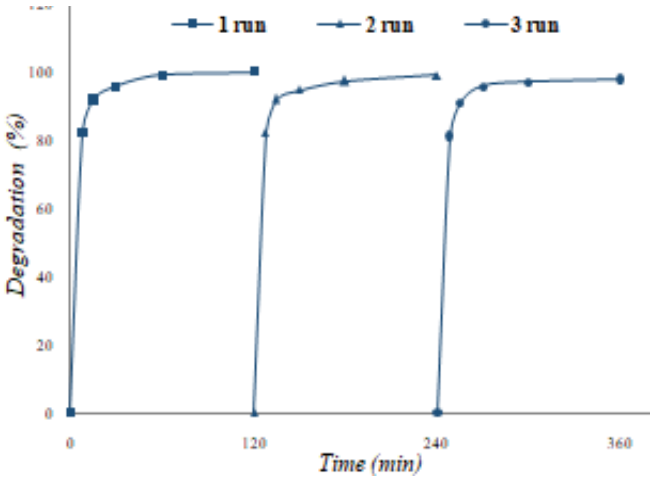

Fig. 13. Degradation efficiency of TIO along the regeneration cycle.

at a low dose of 0.1 g. Therefore, it should be noted that TIO material exhibits photocatalytic activity, which concord well with PL analysis (Fig. 12b) indicating that TIO presents emission band at 550 nm. It can be seen that PL emission intensity of the TIO sample is considered minor. According to Li et al. [40] material with lower PL intensity has less recombination of photo-induced electron-hole pairs. Hence when the recombination rate decreases, more photo-generated charge carriers can participate in the photochemical transformation, resulting in an enhancement in photocatalytic activity [41].

In the presence of H_2O_2, a greater enhancement in photo-Fenton degradation was achieved, resulting in an almost complete mineralization of CR within 1 h.

3.5.2. Adsorbent reusability and stability

Considering the environmental and economic benefits, recycling tests were conducted to evaluate the stability of the iron ores adsorbent during successive adsorption tests and photo-Fenton regenerative reactions in a continuous process. The adsorbent used in the previous test was recovered by centrifugation, washed several times with distilled water, and then dried at 70°C for 24 h. 0.1 g mass of this adsorbent was taken into consideration for each test. The activity of this material is evaluated three times by addition of a fresh dye solution with the recovered adsorbent of the preceding test under these operating conditions: $[CR]_0 = 10^{-4}$ mol L^{-1}, $[H_2O_2]_0 = 10$ mmol L^{-1}, $pH_0 = 7$, and $T = 25$°C.

Fig. 13 displays the regeneration cycles for the photo-Fenton process. Results show that no significant decrease in the adsorption capacity of TIO following three consecutive adsorption–regeneration sequences when drive at natural pH (pH = 7): the % degradation of 96% against 100% at the time of the first use. During these three cycles, the amount of iron passed into solution is measured by atomic absorption. Results show an amount of 3.2 mg L^{-1} noted at closing stages of cycle 1 which increases to 5.67 mg L^{-1} for cycle 3, which explains the slight decreased in the degradation percent noted in cycle 3 (96%), which confirms the stability and the possibility of reusing the iron ore material for the removal of this textile dye.

4. Conclusion

Mined iron oxide (TIO) is a powerful natural abundant and inexpensive catalyst for the mineralization of CR molecule, which is a toxic and carcinogenic diazo dye, very used by textile industries. Physicochemical characterization of TIO (XRD, XRF, and BET) encourage its usefulness as adsorbent material for diazo dye removal from aqueous solution and as a catalyst for its mineralization. Moreover, regeneration experiments with photo-Fenton reaction proved that TIO material had good stability and reusability, demonstrating the feasibility of using this Tunisian material for environmental application. Finally, these pioneering results suggest a further in-depth study for the application of this natural material as a regenerable adsorbent for the removal of several organic compounds in aqueous conditions.

Acknowledgments

The authors would like to extend their sincere appreciation to King Saud University (Riyadh, Saudi Arabia) for the support of this research through Researchers Supporting Project number (RSP-2020/137).

References

[1] M.A. Hassaan, A. El Nemr, Health and environmental impacts of dyes: mini review, Am. J. Environ. Sci. Eng., 1 (2017) 64–67.
[2] A. Pandey, M.P. Singh, S. Kumar, S. Srivastava, Phycoremediation of Persistent Organic Pollutants from Wastewater: Retrospect and Prospects, S. Gupta, F. Bux, Eds., Application of Microalgae in Wastewater Treatment, Springer, Cham, 2019, pp. 207–235.
[3] G. Ghasemzadeh, M. Momenpour, F. Omidi, M.R. Hosseini, M. Ahani, A. Barzegari, Applications of nanomaterials in water treatment and environmental remediation, Front. Environ. Sci. Eng., 8 (2014) 471–482.
[4] C. Wei, F. Zhang, Y. Hu, C. Feng, H. Wu, Ozonation in water treatment: the generation, basic properties of ozone and its practical application, Rev. Chem. Eng., 33 (2017) 49–89.
[5] P.N. Egbuikwem, J.C. Mierzwa, D.P. Saroj, Assessment of suspended growth biological process for treatment and reuse of mixed wastewater for irrigation of edible crops under hydroponic conditions, Agric. Water Manage., 231 (2020) 106003, doi: 10.1016/j.agwat.2020.106034.
[6] N.K. Khanzada, S.J. Khan, P.A. Davies, Performance evaluation of reverse osmosis (RO) pre-treatment technologies for in-land brackish water treatment, Desalination, 406 (2017) 44–50.
[7] E. Rott, R. Minke, H. Steinmetz, Removal of phosphorus from phosphonate-loaded industrial wastewaters via precipitation/flocculation, J. Water Process Eng., 17 (2017) 188–196.
[8] S. Khelifi, F. Ayari, Modified bentonite for anionic dye removal from aqueous solutions. Adsorbent regeneration by the photo-Fenton process, C. R. Chim., 22 (2019) 154–160.
[9] N.H. Singh, K. Kezo, A. Debnath, B. Saha, Enhanced adsorption performance of a novel Fe-Mn-Zr metal oxide nanocomposite adsorbent for anionic dyes from binary dye mix: response surface optimization and neural network modeling, Appl. Organomet. Chem., 32 (2018) 4165, doi: 10.1002/aoc.4165.
[10] M. Bhowmik, M. Kanmani, A. Debnath, B. Saha, Sono-assisted rapid adsorption of anionic dye onto magnetic $CaFe_2O_4$/$MnFe_2O_4$ nanocomposite from aqua matrix, Powder Technol., 354 (2019) 496–504.

[11] C. Srilakshmi, R. Saraf, Ag-doped hydroxyapatite as efficient adsorbent for removal of Congo red dye from aqueous solution: synthesis, kinetic and equilibrium adsorption isotherm analysis, Microporous Mesoporous Mater., 219 (2016) 134–144.
[12] E. Lorenc-Grabowska, G. Gryglewicz, Adsorption characteristics of Congo Red on coal-based mesoporous activated carbon, Dyes Pigm., 74 (2007) 34–40.
[13] R. Zhu, Q. Chen, Q. Zhou, Y. Xi, J. Zhu, H. He, Adsorbents based on montmorillonite for contaminant removal from water: a review, Appl. Clay Sci., 123 (2016) 239–258.
[14] O.S. Omer, M.A. Hussein, B.H. Hussein, A. Mgaidi, Adsorption thermodynamics of cationic dyes (methylene blue and crystal violet) to a natural clay mineral from aqueous solution between 293.15 and 323.15 K, Arabian J. Chem., 11 (2018) 615–623.
[15] Z. Wang, L. Liao, A. Hursthouse, N. Song, B. Ren, Sepiolite-based adsorbents for the removal of potentially toxic elements from water: a strategic review for the case of environmental contamination in Hunan, China, Int. J. Environ. Res. Public Health, 15 (2018) 1653, doi: 10.3390/ijerph15081653.
[16] S. Dandil, D.A. Sahbaz, C. Acikgoz, High performance adsorption of hazardous triphenylmethane dye-crystal violet onto calcinated waste mussel shells, Water Qual. Res. J., 54 (2019) 249–256.
[17] M. Minella, G. Marchetti, E. De Laurentiis, M. Malandrino, V. Maurino, C. Minero, K. Hanna, Photo-Fenton oxidation of phenol with magnetite as iron source, Appl. Catal., B, 154 (2014) 102–109.
[18] H. Bel Hadjltaief, A. Sdiri, M. Gálvez, H. Zidi, P. Da Costa, M. Ben Zina, Natural hematite and siderite as heterogeneous catalysts for an effective degradation of 4-chlorophenol via photo-Fenton process, Chem. Eng., 2 (2018) 29, doi: 10.3390/chemengineering2030029.
[19] A.H. Ltaïef, L.M. Pastrana-Martínez, S. Ammar, A. Gadri, J.L. Faria, A.M. Silva, Mined pyrite and chalcopyrite as catalysts for spontaneous acidic pH adjustment in Fenton and LED photo-Fenton-like processes, J. Chem. Technol. Biotechnol., 93 (2018) 1137–1146.
[20] S. Khelifi, F. Ayari, A. Choukchou-Braham, D.B.H. Chehimi, The remarkable effect of Al–Fe pillaring on the adsorption and catalytic activity of natural Tunisian bentonite in the degradation of azo dye, J. Porous Mater., 25 (2018) 885–896.
[21] M.K. Purkait, A. Maiti, S. Dasgupta, S. De, Removal of Congo red using activated carbon and its regeneration, J. Hazard. Mater., 145 (2007) 287–295.
[22] S. Chawla, H. Uppal, M. Yadav, N. Bahadur, N. Singh, Zinc peroxide nanomaterial as an adsorbent for removal of Congo red dye from waste water, Ecotoxicol. Environ. Saf., 135 (2017) 68–74.
[23] F. Ayari, M.T. Ayadi, Inorganic and organic smectite for synthetic and real textile water treatment. Optical and luminescence properties, Desal. Water Treat., 125 (2018) 47–60.
[24] R. Abidi, N. Slim-Shimi, A. Somarin, M. Henchiri, Mineralogy and fluid inclusions study of carbonate-hosted Mississippi valley-type Ain Allega Pb–Zn–Sr–Ba ore deposit, Northern Tunisia, J. Afr. Earth Sci., 57 (2010) 262–272.
[25] S. Decrée, C. Marignac, T. De Putter, E. Deloule, J.P. Liégeois, D. Demaiffe, Pb–Zn mineralization in a Miocene regional extensional context: the case of the Sidi Driss and the Douahria ore deposits (Nefza mining district, northern Tunisia), Ore Geol. Rev., 34 (2008) 285–303.
[26] S. Bouaziz, E. Barrier, M. Soussi, M.M. Turki, H. Zouari, Tectonic evolution of the northern African margin in Tunisia from paleostress data and sedimentary record, Tectonophysics, 357 (2002) 227–253.
[27] H. Rouvier, V. Perthuisot, A. Mansouri, Pb-Zn deposits and salt-bearing diapirs in Southern Europe and North Africa, Econ. Geol., 80 (1985) 666–687.
[28] C. Savelli, Time–space distribution of magmatic activity in the western Mediterranean and peripheral orogens during the past 30 Ma (a stimulus to geodynamic considerations), J. Geodyn., 34 (2002) 99–126.
[29] N. Sankararamakrishnan, A. Gupta, S.R. Vidyarthi, Enhanced arsenic removal at neutral pH using functionalized multiwalled carbon nanotubes, J. Environ. Chem. Eng., 2 (2014) 802–810.
[30] J. Cai, S. Chen, M. Ji, J. Hu, Y. Ma, L. Qi, Organic additive-free synthesis of mesocrystalline hematite nanoplates via two-dimensional oriented attachment, Cryst. Eng. Commun., 16 (2014) 1553–1559.
[31] F. Ayari, G. Manai, S. Khelifi, M. Trabelsi-Ayadi, Treatment of anionic dye aqueous solution using Ti, HDTMA and Al/Fe pillared bentonite. Essay to regenerate the adsorbent, J. Saudi Chem. Soc., 23 (2019) 294–306.
[32] K.S.W. Sing, Reporting physisorption data for gas/solid systems with special reference to the determination of surface area and porosity (Provisional), Pure Appl. Chem., 54 (1982) 2201–2218.
[33] R. Tanwar, S. Kumar, U.K. Mandal, Photocatalytic activity of PANI/Fe^0 doped BiOCl under visible light-degradation of Congo red dye, J. Photochem. Photobiol., A, 333 (2017) 105–116.
[34] V. Ponnusami, V. Gunasekar, S.N. Srivastava, Kinetics of methylene blue removal from aqueous solution using gulmohar (*Delonix regia*) plant leaf powder: multivariate regression analysis, J. Hazard. Mater., 169 (2009) 119–127.
[35] B. Onida, B. Bonelli, L. Flora, F. Geobaldo, C.O. Arean, E. Garrone, Permeability of micelles in surfactant-containing MCM-41 silica as monitored by embedded dye molecules, Chem. Commun., 21 (2001) 2216–2217, doi: 10.1039/B105261F.
[36] Z. Yermiyahu, I. Lapides, S. Yariv, Visible absorption spectroscopy study of the adsorption of Congo red by montmorillonite, Clay Miner., 38 (2003) 483–500.
[37] C.H. Giles, T.H. MacEwan, S.N. Nakhwa, D. Smith, Studies in adsorption. Part XI. A system of classification of solution adsorption isotherms, and its use in diagnosis of adsorption mechanisms and in measurement of specific surface areas of solids, J. Chem. Soc., 786 (1960) 3973–3993.
[38] I. Langmuir, The adsorption of gases on plane surfaces of glass, mica and platinum, J. Am. Chem. Soc., 40 (1918) 1361–1403.
[39] H.M.F. Freundlich, Uber die adsorption in losungen, zeitschrift fur phtsikalische chemie, Am. Chem. Soc., 62 (1906) 121–125.
[40] P. Li, C. Liu, G. Wu, Y. Heng, S. Lin, A. Ren, W. Shi, Solvothermal synthesis and visible light-driven photocatalytic degradation for tetracycline of Fe-doped $SrTiO_3$, RSC Adv., 4 (2014) 47615–47624.
[41] Y. Shi, Z. Yang, Y. Liu, J. Yu, F. Wang, J. Tong, B. Su, Q. Wang, Fabricating a g-C_3N_4/CuO_x heterostructure with tunable valence transition for enhanced photocatalytic activity, RSC Adv., 6 (2016) 39774–39783.